JTTEE5 10:375-381

The Features of Cold Spray Nozzle Design

A.P. Alkhimov, V.F. Kosarev, and S.V. Klinkov

(Submitted 14 February 2000)

This article presents the peculiarities of the supersonic nozzle design for the cold gas-dynamic spraying. The procedure to produce the high particle velocity by correct choice of the geometrical dimensions of the accelerating nozzles is described. Numerical and experimental research of wedge-shaped nozzles shows that there is a nozzle with its particular dimensions for a given type of particles that produces the maximum possible particle velocity at the moment of impact on a target surface.

Keywords boundary layer, bow shock, cold spray, jet, modeling, nozzle

1. Introduction

One of the main problems in the gas-dynamic spray process is providing the optimal velocity (kinetic energy) of the particles that form the coating.[1] Experimental data show that the efficiency of these dynamic parameters may be raised if we take care of some effects (boundary layer along the nozzle walls and a local high-pressure region) that occur when the gas-powder mixture moves in the supersonic nozzle and when the jet impinges on the substrate. Thus, the consideration of the problems concerning the development of the Laval nozzles applied for the spraying is urgent. Gas-dynamic principles that are at the basis of this article are generally true for all conventional thermal spray techniques that use two-phase gas-particle mixture flows. The common problems for these techniques are the increase of productivity and the lower product costs, *i.e.*, the possibility to rapidly apply the coatings over the larger surface area under the lower gas flow rate and energy consumption conditions. One of the ways to solve this problem is to use flat two-phase jets of small thickness. This decreases the carrier gas consumption and allows more even material deposition. This article is dedicated to the design and study of the nozzle shapes that produce these jets.

Figure 1 shows the shape and geometrical dimension nomenclature of these nozzles. Expansion from the nozzle throat to the outlet cross section is assumed to be proportional to the axial coordinate, *i.e.*, the angle of the nozzle generator slope to the nozzle axis is constant. These nozzles are easily produced and make it possible to vary one of the dimensions of spray spot and obtain the minimum possible spray spot size that is necessary in some cases of the practical application.

The particle velocity increase is known to result in better coating quality, as demonstrated by high-velocity spray methods and devices (HVOF, JP5000, and CGS). Therefore, designed nozzles should provide high particle velocities.

The basic gas-dynamic principles of the cold spray nozzle design are presented in Ref 2. A brief description of the setup scheme, coating properties, and advantages and limitations of the cold spray method are given there. However, some phenomena that influence essentially the gas dynamics and are important for the accelerating nozzle design are paid negligible regard in Ref 2. These are the presence of the boundary layer along the nozzle walls and the low-velocity subsonic high-pressure region that occurs in front of the target surface while the supersonic two-phase jet impinges on the substrate.

A.P. Alkhimov, V.F. Kosarev, and S.V. Klinkov, Institute of Theoretical and Applied Mechanics SB RAS, Novosibirsk, Russia. Contact e-mail: alkh@itam.nsc.ru.

2. Internal Gas Motion

To accelerate particles in the nozzle up to the gas velocity, it is necessary to increase the nozzle length L. However, as the nozzle length increases, the boundary layer thickness increases. This leads to the decrease of the effective nozzle cross-sectional area downstream in comparison to the geometrical cross-sectional area. As a result, the gas velocity decreases at the nozzle exit in comparison to the ideal gas flow velocity.

2.1 Modeling Gas Motion

Now we consider the gas motion model inside the rectangular supersonic nozzle. The model proposed consists of two different parts that are divided by boundary layer meeting.

Before Meeting. When the boundary layer thickness is small enough, the gas parameters in a flow core near the nozzle axis vary according to the isentropic formulas. However, increasing along the wall, the boundary layer decreases the cross section of the cannel by the value $\delta^* U$, where δ^* is the displacement thickness usually defined by the expression

$$\delta^* = \int_0^{h/2} \left(1 - \frac{\rho v}{\rho_m v_m}\right) dy \qquad \text{(Eq 1)}$$

The displacement thickness has proper physical sense. It is a distance by which streamlines of external current are departed from the wall owing to a diminution of a velocity in the boundary layer. The displacement thickness δ^* is calculated with the aid of Karman (Eq 2) from[3]

$$\frac{d\delta^{**}}{dz} = \frac{c_f}{2} - \frac{\delta^{**}}{v_m}\frac{dv_m}{dz}\left(2 + H_2 - \mathrm{M}^2\right) dy \qquad \text{(Eq 2)}$$

$$\delta^* = \delta^{**} H_2 \qquad \text{(Eq 3)}$$

where δ^{**} is the momentum thickness, defined by the expression

Nomenclature

a	gas sound speed
A_c	nozzle throat area
c_p	constant pressure specific heat
C_D	drag coefficient
c_f	friction coefficient
d_p	particle diameter
G	gas flow rate
M	Mach number at the nozzle axis
M*	Mach number at the nozzle exit
M_G	Mach number of isentropic gas flow at the nozzle exit
M_S	Mach number after bow shock
M_p	particle Mach number
$\overline{M}$	averaged Mach number
m_p	particle mass
n	exit pressure ratio, *i.e.*, the ratio of pressure at nozzle exit and ambient pressure
p	pressure
p_0	stagnation pressure
R	specific gas constant
Re_z	Reynolds number based on z
Re_p	particle Reynolds number
S	area of the nozzle cross section
S_{mid}	cross-sectional area of the particle
T	gas temperature
T_0	stagnation temperature
U	perimeter of the nozzle cross section
v	gas velocity
v_p	particle velocity
v_{pw}	impact particle velocity
v*	gas velocity at the nozzle exit
$\overline{V}$	averaged gas velocity
v_m	axial velocity
y	coordinate counted off from the wall to the nozzle axis
z	coordinate along the nozzle axis
z_w	compressed layer thickness
z_0	stand-off distance

Greek symbols

γ	specific heats ratio
δ	boundary layer thickness
δ*	displacement thickness
δ**	momentum thickness
μ	viscosity
ρ	gas density
ρ_m	gas density at nozzle axis
ρ_p	density of particle material
$\overline{\rho}$	averaged gas density

$$\delta^{**} = \int_0^{h/2} \frac{\rho v}{\rho_m v_m}\left(1 - \frac{v}{v_m}\right)dy \qquad \text{(Eq. 4)}$$

and having here auxiliary significance. There is a relation between δ* and δ** in accordance with formula 3.

Dependence on the Mach number of the ratio between the displacement thickness and the momentum thickness H_2 was determined by formula 5 from Ref 4, which is an approximation of experimental data:

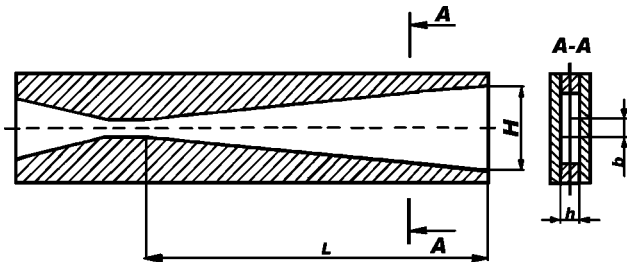

Fig. 1 Outward shape of investigated nozzles and applied notation of parameters

$$H_2 = 1.4(1 + 0.3M^2) \qquad \text{(Eq 5)}$$

The friction coefficient c_f is calculated according to expressions 6 to 9 from Ref 5.

$$c_f = c_{f0}\frac{1-\xi}{\xi}\arcsin^2\sqrt{\xi} \qquad \text{(Eq 6)}$$

$$c_{f0} = 0.0263\,\mathrm{Re}_z^{-1/7} \qquad \text{(Eq 7)}$$

$$\mathrm{Re}_z = \frac{\rho v z}{\mu} \qquad \text{(Eq 8)}$$

$$\xi = \frac{\frac{\gamma-1}{2}M^2}{1+\frac{\gamma-1}{2}M^2} \qquad \text{(Eq 9)}$$

Formula 6 contains two parts. In the first part, c_{f0}, defined by Eq 7 and 8, is a friction coefficient for low velocity flows. The second part is entered into the formula to take into account the friction dependence on the Mach number. The viscosity γ is calculated by the Sutherland formula.[3]

The calculations are performed as follows. In the first step, axial gas parameters are found according to isentropic formulas. Second, the displacement thickness is found according to the Karman equation. Then, new values of nozzle cross-sectional area are found by subtracting the calculated displacement thickness from the nozzle geometrical dimensions. Further, in accordance with the first step, new axial gas flow parameters are found. The process rapidly converges to the only possible values of the axial parameters and displacement thickness.

Registration of the increase in the boundary layer thickness, hence, the integration of the Karman equation, may start with the Laval nozzle throat because the highly convergent flow occurs in the subsonic part of a small length and the boundary layer thickness is negligible here.

This model is limited by a condition of boundary layer junction. Using δ* and M, the boundary layer thickness may be estimated by formula 10 from Ref 6.

$$\frac{\delta^*}{\delta} = 1 - 7\int_0^1 \frac{\zeta^7 d\zeta}{1+\frac{\gamma-1}{2}M^2(1-\zeta^2)} \qquad \text{(Eq 10)}$$

where ζ is the formal variable parameter of integration.

The calculated δ compares with one-half of the nozzle thickness $h/2$. The boundary layer meeting is obvious under condition $\delta = h/2$. Then, the model presented here becomes incorrect because of invalidation of isentropic formulas near the nozzle axis.

After Meeting. When the boundary layers meet, the gas flow is reconstructed downstream. This reconstruction means that the velocity profile obtains the shape that is described by one independent on the longitudinal coordinate z law. Flows of this kind usually are named as automodel or self-similar flows. In this case, calculation is executed according to Eq 11 to 15 for the gas flow parameters averaged over the nozzle cross section (marked here by a dash above the symbol)

$$G = \bar{\rho}\bar{v}S = \text{const} \quad \text{(Eq 11)}$$

$$G\frac{d\bar{v}}{dz} = -S\frac{dp}{dz} - F_f \quad \text{(Eq 12)}$$

$$Gc_p\frac{d\bar{T}}{dz} = \frac{G}{\bar{\rho}}\frac{dp}{dz} + \bar{v}F_f \quad \text{(Eq 13)}$$

$$p = \bar{\rho}R\bar{T} \quad \text{(Eq 14)}$$

$$F_f = \frac{1}{2}c_f\overline{\rho v^2}U \quad \text{(Eq 15)}$$

In the case of constant stagnation temperature, this system may be reduced to one equation:

$$\frac{d\overline{M}}{dz} = \overline{M}\frac{1+\frac{\gamma-1}{2}\overline{M}^2}{\overline{M}^2-1}\left(\frac{dS}{dz} - \frac{1}{2}c_f\overline{M}^2U\right) \quad \text{(Eq 16)}$$

The gas velocity profile is expressed by the widely known approximation 17 from Ref 3.

$$\frac{v}{v_m} = \left(\frac{y}{\delta}\right)^{1/7} \quad \text{(Eq 17)}$$

where $\delta = h/2$. An illustrative picture is presented in Fig. 2. Proceeding from this, it is easy to obtain the relations of averaged and axial flow parameters. Velocity averaging performs according to formula 18,

$$\bar{v} = \frac{1}{S}\int v dS \quad \text{(Eq 18)}$$

and, in the case of the rectangular nozzle, reduces to the expression

$$\bar{v} = v_m\int_0^{\delta}\left(\frac{y}{\delta}\right)^{1/7} d\left(\frac{y}{\delta}\right) = \frac{7}{8}v_m \quad \text{(Eq 19)}$$

Other averaged parameters are originated from the law of gas flow rate conservation,

$$\bar{\rho} = \frac{G}{\bar{v}S} \quad \text{(Eq 20)}$$

and perfect gas state equation:

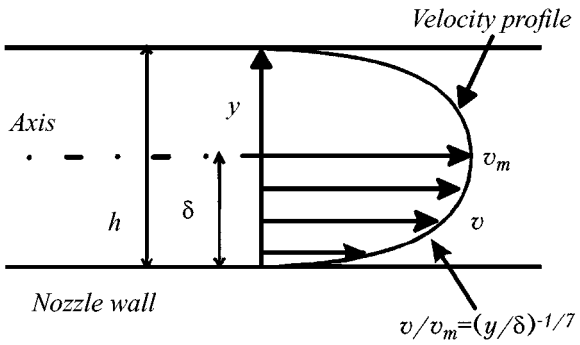

Fig. 2 Auxiliary picture to velocity profile approximation inside the nozzle by "1/7" law

$$\bar{T} = \frac{p}{\bar{\rho}R} \quad \text{(Eq 21)}$$

The pressure does not vary across the boundary layer, *i.e.*, $\bar{\rho} = \rho$. Written-out relationships make it possible to complete the gas flow model inside the nozzle.

Thus, the main governing statutes of the suggested gas flow model within the nozzle are as follows. In the subsonic part of the nozzle, the calculation is performed according to the ideal gas model. From the nozzle throat, the increase of boundary layers along the nozzle walls is numerically determined by the Karman equation up to the point where boundary layers meet. In this case, the stagnation pressure near the nozzle axis is preserved. Then, starting from the point of the boundary layers' junction, the automodel (self-similar) gas flow appears, and calculation is performed by equations for the mean gas flow parameters. Axial parameter values are restored in accordance with the "1/7" velocity distribution law.

In general, more accurate models can be used. However, this model is simple enough and permits quick acquisition of the estimates of the gas parameters near the nozzle axis at any axis point within the nozzle.

2.2 Verification

To check the calculation correctness of the mentioned model, the axial Mach number values at the nozzle exit were measured. Figure 3 shows the ratio of the real Mach number M* obtained by either calculation or experiment and the Mach number M_G that should exist when the boundary layer along the nozzle walls is absent. This ratio is presented versus the ratio of the nozzle thickness and the nozzle length.

The calculation is performed for three different Mach numbers: $M_G = 2.18$, 2.72, and 3.45. The ration h/L is varied in three different ways:

- varying L from 20 to 300 mm at constant other dimensions but different Mach numbers and stagnation pressure (numbers 3 and 4 in Fig. 3 mark these results);
- varying h from 1 to 10 mm at constant other dimensions, marked by 2; and
- varying L at the proportional varying b and H (number 1 corresponds to $b = 0.03L$ and $H = 0.01L$).

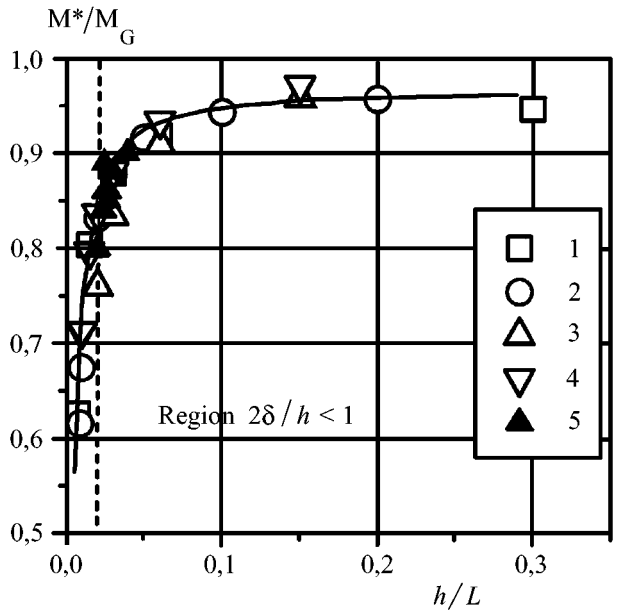

Fig. 3 Dependency of the relative Mach number at the nozzle exit on relative extension of the nozzle. (1) $M_G = 2.72$, $p_0 = 1.5$ MPa, $h = 3$ mm, $b/H = 0.3$, and $h/L = 0.03$; (2) $M_G = 2.72$, $p_0 = 1.5$ MPa, $L = 0.1$ m, $b = 3$ mm, and $H = 10$ mm; (3) $M_G = 2.18$, $p_0 = 0.6$ MPa, $h = 3$ mm, $b = 3$ mm, and $H = 6$ mm; (4) $M_G = 3.45$, $p_0 = 1.5$ MPa, $h = 3$ mm, $b = 3$ mm, and $H = 20$ mm; and (5) $M_G = 2.0$ to 3.35, experimental results

As a result, the values of the nozzles were calculated in the following ranges: $h = 1$ to 10 mm, $L = 20$ to 300 mm, and $H = 2$ to 30 mm. This great calculation volume was performed for the purpose of showing that the data are well generalized in the given coordinates. All points sit near the single curve in spite of different calculation conditions. Also, the experimental data points (number 5 in Fig. 3) sit at the same curve.

It should be noted that, when h/L approaches infinity, the ratio M^*/M_G tends to unity. It means physically that, with the decrease of the nozzle length at constant thickness or with the increase of the thickness at constant length, the influence of the boundary layer on the main gas flow vanishes and the gas flow acquires the features of the ideal gas flow.

The investigation carried out allows us to use Fig. 3 for rapid practical estimates. For example, if we produce the nozzle at $h/L = 0.02$, then we should wait for the nozzle exit Mach number to be lowered to $0.85M_G$ independent of the p_0 and M_G. Moreover, Fig. 3 also shows that the boundary layers meet at a h/L of about 0.02 (dashed line).

In Fig. 3, two regions are presented. When the nozzle is short, the boundary layers do not meet. This region (singed as region $2\delta/h < 1$) sits on the right side of Fig. 3. The other region (that sits on left side of Fig. 3) corresponds to the long nozzles, when boundary layers meet. Physically, the meeting means that stagnation pressure near the nozzle axis starts to decrease because of friction on the wall. It is reflected in Fig. 3 by the following case: if h/L tends to zero, then M^*/M_G decreases.

The results presented here prove that the nozzle lengthening for the best particle acceleration purposes at a given nozzle thickness is limited by an increase of the boundary layers along the nozzle walls. To diminish the boundary layer influence under a constant nozzle length condition, it is necessary to increase the nozzle thickness. However, it is shown later also to be limited.

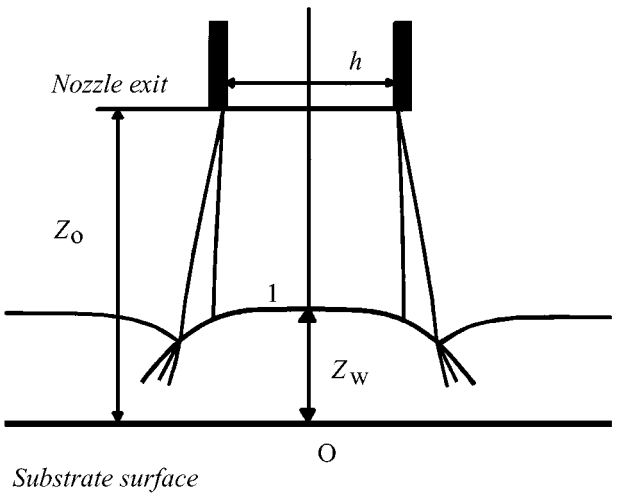

Fig. 4 The scheme of supersonic gas jet impingement on flat unrestricted obstacle. 1 = detached shock, h = nozzle thickness, and z_0 = distance from nozzle exit to an obstacle

3. Jet Impingement

Let's consider a supersonic jet impingement on the normally positioned obstacle (Fig. 4). A deceleration and turning of a gas flow occur in front of an obstacle surface. The transition from a high-velocity supersonic flow to a low velocity subsonic one occurs by the shock that appears at some distance z_w from the obstacle surface. A high-pressure and high-density gas layer is created between the obstacle surface and the shock. Apparently, small particles of the deposited material coming through this compressed layer will lose some of their velocity. This quantity becomes greater the greater is the compressed layer thickness.

3.1 Compressed Layer Thickness

It follows from the above discussion that, for an estimate of particle velocity loss when it moves through the compressed layer, it is necessary to determine the compressed layer thickness and Mach number distribution inside the compressed layer.

Using the gas mass balance law written for the case of the rectangular cross section jet impingement, it is possible to obtain the next relationship:

$$z_w = k\frac{h}{1 + h / H} \qquad \text{(Eq 22)}$$

Factor k is introduced into the formula for the purpose of taking into account the gas density varying within the compressed layer. To determine the compressed layer thickness, several experiments were carried out. The aim of the experiments was to obtain k. The standoff distance, Mach number, nozzle thickness, and pressure ratio n alter through the experiments. Figure 5 shows the results of these experiments. The plotted ordinate is a

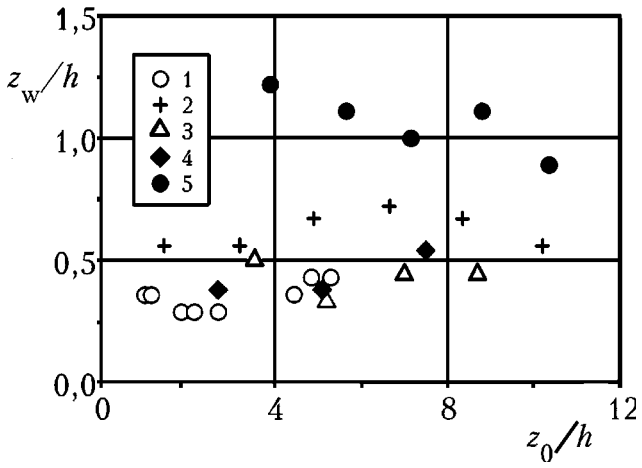

Fig. 5 Dependency of compressed layer thickness on distance. The total range of varied parameters was $h = 1$ to 5 mm, $H/h = 2.7$ to 8, and M = 1.8 to 3.1. Dark circles denote data for $n = 3$, and the remainder are $n = 1$. (1) $h = 3$ mm, $H = 8$ mm, and M = 2.1; (2) $h = 1$ mm, $H = 8$ mm, and M = 1.8; (3) $h = 3$ mm, $H = 10$ mm, and M = 1.8; (4) $h = 4.5$ mm, $H = 12$ mm, and M = 3.1; and (5) $h = 3$ mm, $H = 10$ mm, M = 1.8, and $n = 3$

compressed layer thickness and the plotted abscissa is a standoff distance z_0. These parameters are both dimensionalized by the geometrical nozzle thickness. We can see that, in given coordinates, the data are not generalized. The pressure ratio n strongly influences the compressed layer thickness (number 5 in Fig. 4). However, if we consider only isobaric exhaustion (numbers 1 to 4), then, as a first approximation step, the averaged constant value k may be obtained. It is a very rough approximation. To obtain a more accurate approximation, it is necessary to apply a more accurate model of jet stream and impingement. However, until now, there has been no simple model that would allow all of the above-mentioned parameters to change in a wide range. This is complicated also by the appearance of nonstationary phenomena as oscillations of jet and bow shock at nonisobaric exhaustion. The investigation of these flows is quite difficult and will not be discussed here. The purpose of this article is satisfied by accepting k as being equal to 0.4660.01 according to experimental data averaging. Thus, our research area is restricted by isobaric exhaustion consideration.

3.2 Mach Number Variation

Determination of the Mach number distribution inside the compressed layer thickness is also quite difficult. Here, we use the widely known cunning method of polynomial approximation between the two points at the Mach numbers, and their derivations are defined. The temporary point of reference is chosen to be at the position of the shock at the jet axis. A polynomial of third order satisfies the following boundary conditions 23 and 24.

After the shock, $z = 0$:

$$M = M_s \text{ and } dM/dz = 0 \quad \text{(Eq 23)}$$

On the surface, $z = z_w$:

$$M = 0 \text{ and } dM/dz = -0.5M_s/z_w \quad \text{(Eq 24)}$$

Most of them are obvious. The last condition is derived from the generalization of a great number of experimental data[7,8] and denotes that the velocity gradient at the point of a flow turn (point O in Fig. 4) is uniform. To be uniform here means that velocity gradients are equal according to the velocity circulation conservation theorem at the point O, *i.e.*, $\left|\frac{\delta M}{\delta y}\right| = \left|\frac{\delta M}{\delta z}\right|$. We can replace v with M because v tends to zero at point O. The following dependency satisfies the boundary conditions mentioned above:

$$M = M_s\,(1.5(z/z_w)^3 - 2.5\,(z/z_w)^2 + 1) \quad \text{(Eq 25)}$$

Thus, concluding this section, the compressed layer thickness depends on the main governing parameter, which is the nozzle thickness. As seen from Eq 22, the compressed layer thickness increases when the nozzle thickness h is set to the greater value and when the ratio h/H remains the same. As a consequence, it leads to the increasing loss of the particle velocity of the deposited material. This fact alone hinders the choice of the greater thickness of designed nozzles for reducing the influence of the boundary layers.

4. Particle Motion

The solution of the nozzle optimization problem is impossible without a particle motion model. In this section, we consider in more depth the particle motion model used and discuss some results of the experimental particle velocity definition.

4.1 Particle Motion Modeling

To calculate the particle velocity v_p, the model of the single particle motion is used. It allows us to disregard the influence of particles on the gas flow parameters. The application of the single particle model is known to be justified by low powder loading the gas flow (volume concentration of particles less than 10^{-6} to 10^{-4}) that is often used in practice. The volume concentration is defined as the ratio between the volume of all particles and the entire volume. Thus, this parameter is dimensionless. It is supposed that the particles move along the nozzle axis and along the jet axis. Particle velocity was calculated by Eq 26 to 28:

$$m_p v_p \frac{dv_p}{dz} = C_D \frac{\rho(v - v_p)^2}{2} S_{\text{mid}} \quad \text{(Eq 26)}$$

$$M_p = \frac{v - v_p}{a} \quad \text{(Eq 27)}$$

$$Re_p = \frac{(v - v_p)\rho d_p}{\mu} \quad \text{(Eq 28)}$$

The gas parameters are taken near the axis. The drag coefficient C_D is calculated by the Henderson approximation.[9]

4.2 Verification

To check the calculation correctness, the particle velocity at the nozzle outlet was determined experimentally.

There is a problem with selecting the parameters that generalize computational and experimental data. For plotting the par-

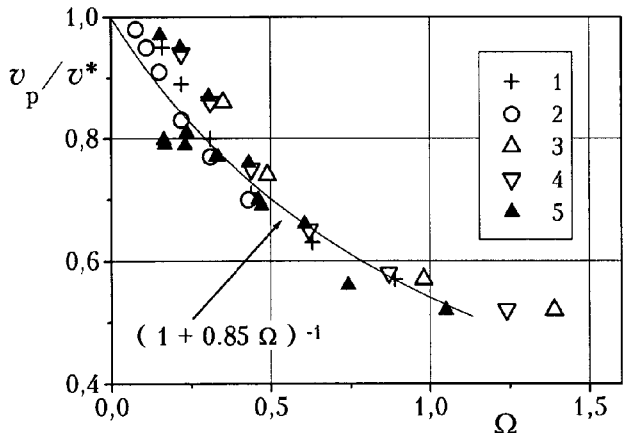

Fig. 6 Generalized dependency of relative particle velocity at outlet of the flat supersonic nozzle. (1) $L = 50$ mm, $p_0 = 1.5$ MPa, and $T_0 = 300$ K, Al; (2) $L = 100$ mm, $p_0 = 3.0$ MPa, and $T_0 = 300$ K, Al; (3) $L = 50$ mm, $p_0 = 1.0$ MPa, and $T_0 = 500$ K, Cu; (4) $L = 100$ mm, $p_0 = 3$ MPa, and $T_0 = 500$ K, Cu; and (5) experimental results, Al and Cu

ticle velocity at the nozzle exit, we have chosen the ratio of particle velocity and gas velocity at the nozzle exit, and also a complex Ω (Eq 29), which, under our judgement, characterizes all binders according to Eq 26:

$$\Omega = (d_p/L)^{0.5}(\rho_p v_*^2/p_0)^{0.5} \quad \text{(Eq 29)}$$

From the analyzing ratio (Eq 29), it is easily seen that the parameters standing above in a numerator compensate for the effect of parameters standing in a denominator. For example, the particle size increase is compensated for by either nozzle length or stagnation pressure increase. This same situation holds for the particle density. To make this complex dimensionless, it is necessary to enter some characteristic speed into it. We used gas velocity at the nozzle exit as the characteristic speed. Thus, the plot presented in Fig. 6 maps the data generally, *i.e.*, the chosen axis labels allow a relationship to be presented by one law. We approximate this law by the formula

$$\frac{v_p}{v^*} = \frac{1}{1 + 0.85\,\Omega} \quad \text{(Eq 30)}$$

To find the range of the law applicability, the various change versions of parameters included in the complex Ω were calculated. Appropriate numbers from 1 to 4 mark these versions in Fig. 6. The total range of parameters was $L = 50$ to 150 mm, $p_0 =$ 1 to 3 MPa, $T_0 = 300$ to 500 K, particle density $2.7 \cdot 10^3$ to $9 \cdot 10^3$, and particle size from 5 to 80 μm. Figure 6 also provides a prediction of particle velocity at the nozzle outlet. First, the gas velocity at the nozzle exit is obtained with the aid of Fig. 3. Then, complex Ω is calculated using this gas velocity. Finally, particle velocity estimates are made using Ω and v^* in accordance with Fig. 6.

In Fig. 6, the experimental data marked by number 5 are also shown. These experimental data sit at the same curve as well as computation. This proves that the computational model described above quite adequately reflects reality, *i.e.*, is reliable. It allows application of the model to the solution of the optimization problem.

5. Optimization Problem

To determine the particle motion parameters in the jet, the gas parameters were assumed to be the same as the values at the nozzle outlet. Under the condition of the cold gas-dynamic spray process, this simplification is justified because the standoff distances are small. The last statute allows completion of the particle motion model along the entire gas-dynamic path and the onset of the search for the optimal nozzle parameters.

It follows from the above discussion that the nozzle optimization problem must be considered as the particle velocity maximization not at the point of nozzle outlet but at the point of contact with a target surface v_{pw}. Then, the thickness of the flat nozzles (or the diameter of the axisymmetric nozzles) and the nozzle length are both the most important parameters.

To obtain optimal values of the nozzle thickness and nozzle length, we set the next limitations. The stagnation (total) temperature of gas is constant (the case of heat insulated nozzle walls). The throat areas A_c and the values of stagnation pressure at the nozzle inlet p_0 are the same for the different nozzles.

These constraints make the gas flow rate in the different nozzles the same. Thus, we have considered the optimization problem as it regards the variety of wedge-shaped nozzles of equal gas flow rate producing the isobar jets.

The calculation is executed as follows. Particle size and density, and also p_0, T_0, and A_c, are set as constant parameters during numerical searching for optimal h and L. The value of b is obtained using the formula

$$A_c = bh \quad \text{(Eq 31)}$$

It was supposed that the jet exhausts in a chamber where the pressure is $1 \cdot 10^5$ Pa. To make the pressure in the exhausted jet equal to that in the ambient one (isobar exhaustion), a greater dimension of the nozzle cross section at the nozzle exit H was chosen.

Further, setting different h and L values, we may obtain massive $v_{pw}(h, L)$. By comparison of the obtained values of the particle velocity at impact $v_{pw}(h, L)$, the velocity's maximum value and the values of the optimal parameters were found.

Figure 7 presents a typical graph of isolines of the particle velocities at impact $v_{pw}(h, L)$. It is seen that curves are concentrated around one region where the particle velocity obtains a maximum value (in Fig. 7, this region is bordered with an isoline of 580 m/s). This denotes that the maximum impact velocity can only be produced by applying the nozzle when the values of the length and thickness are precisely given.

Unfortunately, we did not have the opportunity to test experimentally the particle velocity at impact with a surface. Thus, we relied upon the results of the calculations. These calculations, however, were tested experimentally at some stages, which makes them reliable.

6. Conclusions

As we can conclude from the present article, there is a nozzle of definite dimensions for a certain type of particles that can pro-

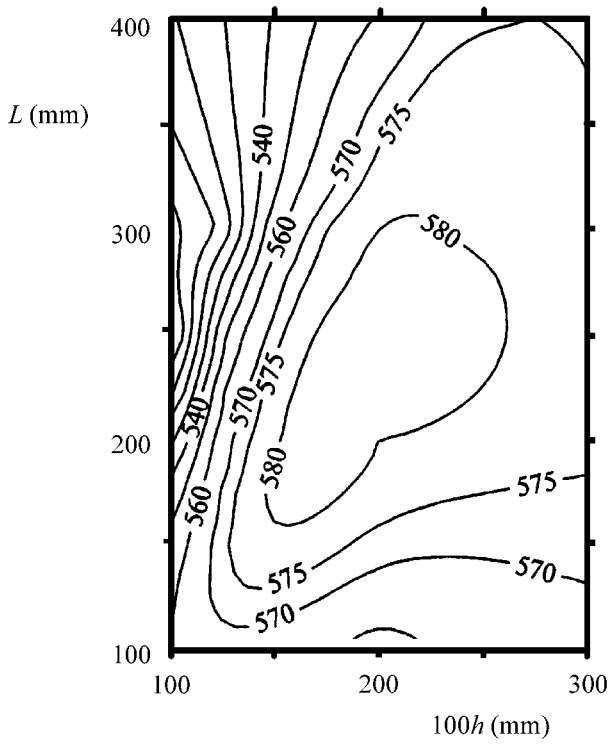

Fig. 7 Isolines of velocity of aluminum particles $d_p = 10$ μm at impact on the surface of an obstacle ($z_0 = 15$ mm, $T_0 = 470$ K, and $p_0 = 1.5$ MPa). Numbers on the curves denote values of impact velocity, m/s

vide the maximum impact velocity of particles on a substrate surface.

We should note that the approach presented here opens an opportunity for the spraying of the ultradispersive powders ($d_p =$ 0.01 to 0.5 μm) in contradistinction to the traditional estimates of the impact velocity by the velocity at the nozzle outlet. These estimates are not useful because the particles of such a small size form a velocity balance two-phase flow of the small relaxation length. This means that the impact particle velocity is also very small. Otherwise, applying the approach described above, it is possible to get the most favorable condition for the ultradispersive powder spraying.

Thus, it has been shown that the effects of boundary and compressed layers not considered before have a sufficient influence on the final particle velocity; the smaller the size of the particles, the greater is their influence. This influence should be taken into account especially in the case of the cold spray nozzle design, because the particle size of the commonly used powders is small and the impact particle velocity is very important.

The solution suggested here is thought to yield the optimal nozzle dimensions and impact particle velocity and, therefore, to forecast the behavior of the heterogeneous jet-obstacle interaction.

References

1. A.P. Alkhimov, V.F. Kosarev, and A.N. Papyrin: *Dokl. Akad. Nauk SSSR*, 1990, vol. 315 (5), pp. 1062-65.
2. R.C. Dykhuizen and M.F. Smith: *J. Thermal Spray Technol.*, 1998, vol. 7 (2), pp. 205-12.
3. G. Schlichting: *Nauka, Moscow*, 1969, p. 742 (in Russian).
4. M.E. Deich and A.E. Zaryankin: *Energiya, Moscow*, 1970, p. 384 (in Russian).
5. L.G. Loitsyanski: *Nauka, Moscow*, 1970, p. 904 (in Russian).
6. G.N. Abramovich: *Nauka, Moscow*, 1969, p. 824 (in Russian).
7. I.A. Belov, I.P. Ginzburg, and L.I. Shoob: *Int. J. Heat and Mass Transfer*, 1973, vol. 16, pp. 2067-76.
8. T. Nakatogawa, M. Hirata, and I. Kukita: *J. Spacecraft*, 1971, vol. 8 (4), pp. 410–11.
9. C.B. Henderson: *AIAA J.*, 1976, vol. 14, pp. 707-08.